

Free vibration analysis of laminated plate/shell structures based on FSDT with a stabilized nodal-integrated quadrilateral element

H. Nguyen-Van^a, N. Mai-Duy^a, T. Tran-Cong^{a,*}

^a*Computational Engineering & Science Research Centre (CESRC), Faculty of Engineering and Surveying, University of Southern Queensland, Australia*

Abstract

This paper reports numerical analyses of free vibration of laminated composite plate/shell structures of various shapes, span-to-thickness ratios, boundary conditions and lay-up sequences. The method is based on a novel four-node quadrilateral element, namely MISQ20, within the framework of the first-order shear deformation theory (FSDT). The element is built by incorporating a strain smoothing method into the bilinear four-node quadrilateral finite element where the strain smoothing operation is based on mesh-free conforming nodal integration. The bending and membrane stiffness matrices are based on the boundaries of smoothing cells while the shear term is evaluated by 2×2 Gauss quadrature. Through several numerical examples, the capability, efficiency and simplicity of the element are demonstrated. Convergence studies and comparison with other existing solutions in the literature suggest that the present element is robust, computationally inexpensive and free of locking.

Key words: free vibration, laminated plate/shell, strain smoothing method, shear-locking free, first-order shear deformation theory.

1 Introduction

The analysis of natural frequencies of composite plates/shells plays an increasingly important role in the design of structures in mechanical, civil and

* Correspondence to: T. Tran-Cong, CESRC, USQ, Toowoomba, QLD 4350, Australia, Tel. +61 7 46312539, Fax. +61 7 46312526.

Email address: trancong@usq.edu.au (T. Tran-Cong).

aerospace engineering applications. A thorough study of the dynamic behaviors of these structures is essential in assessing their full potential. Therefore, it is necessary to develop appropriate models capable of accurately predicting their dynamic characteristics.

Great progress has been made over past decades towards better understanding of the vibration characteristics of laminated composite plates/shells [1, 2, 3]. Due to limited availability of analytic solutions for practical applications, numerical approximate methods have become the most effective tools. The finite element method (FEM) is considered to be a very effective and versatile approach for these problems. There is a vast amount of literature on free vibration analysis of laminated plates/shells which is too large to list here. Bert [1] and Mohamad [2] have conducted surveys and provided details on the development of the finite element methods for modeling and modal analysis of laminated plates/shells. Further extensive references on shells can be found in the excellent review of Yang *et al.* [3].

Although the FEM solution is quite effective and versatile, its performance is highly mesh dependent and badly deteriorates when mesh distortion occurs. On the other hand, the mesh-free methods have become an alternative approach for problems with complex geometry and boundary conditions. Several mesh-free methods have been so far proposed for vibration analysis, including the Element Free Galerkin method (EFG) [4], the Moving Least Square Differential Quadrature method (MLSDQ) [5, 6], the Radial Basis Function method (RBF) [7, 8] and the Reproducing Kernel Particle method [9], etc. However, the complex approximation space of mesh-free methods increases the computational cost of solving the resultant algebraic equation systems. Recently, Liu *et al.* [10, 11] proposed a new smoothed finite element method (SFEM) where the strain smoothing technique of the stabilized conforming nodal integration (SCNI) mesh-free method was incorporated into the existing FEM for 2D elastic problems. Based on the idea of SFEM, Nguyen-Van *et al.* [12] have developed a new locking-free quadrilateral laminated plate element MISQ20 by incorporating the SCNI into the Bathe-Dvorkin assumed strain plate element [13]. It is found that the MISQ20 element with SCNI is effective, computationally inexpensive and not sensitive to mesh distortion. It is able to achieve accurate results even with coarse discretization irrespective of the span-to-thickness ratio and stacking sequence.

The goal of the present study is to extend the MISQ20 element for analysis of free vibration problems of laminated plate/shell structures within the framework of the FSDT. Eigenvalue analysis of various composite plates/shells is performed in order to have a better understanding of their dynamic behaviors associated with different parameters such as boundary conditions, types of laminates, mesh distortion, fibre orientation, span-to-thickness ratio, mixed boundaries and modulus ratio.

The paper is outlined as follows. First, a brief review of the finite element formulations for laminated plates is introduced in section 2. The description of strain smoothing technique for finite element method is derived in section 3. Several numerical investigations are carried out in section 4 to assess the performance of the proposed element in free vibration analysis. Finally, concluding remarks are made in section 5.

2 Finite element formulations for laminated plates

In the first-order shear deformation theory (FSDT) [14], the plate kinematics is governed by the midplane displacement u_o, v_o, w_o and rotation θ_x, θ_y as follows.

$$\begin{aligned} u(x, y, z) &= u_o(x, y) + z\theta_x, \\ v(x, y, z) &= v_o(x, y) + z\theta_y, \\ w(x, y, z) &= w_o(x, y). \end{aligned} \quad (1)$$

A typical 4-node quadrilateral laminated plate element consisting of n layers with thickness h is shown in Figure 1.

The in-plane strain vector $\boldsymbol{\varepsilon} = [\varepsilon_x \quad \varepsilon_y \quad \varepsilon_{xy}]^T$ can be rewritten as

$$\boldsymbol{\varepsilon} = \begin{bmatrix} u_{o,x} \\ v_{o,y} \\ u_{o,y} + v_{o,x} \end{bmatrix} + z \begin{bmatrix} \theta_{x,x} \\ \theta_{y,y} \\ \theta_{x,y} + \theta_{y,x} \end{bmatrix} = \boldsymbol{\varepsilon}_m + z\boldsymbol{\varepsilon}_b, \quad (2)$$

and the transverse shear strain vector as

$$\boldsymbol{\gamma} = [\gamma_{xz} \quad \gamma_{yz}]^T = [\theta_x - w_{,x} \quad \theta_y - w_{,y}]^T. \quad (3)$$

For an anisotropic laminated plate, the stress and resultant constitutive relationship are expressed as follows.

$$\boldsymbol{\sigma}_p = \begin{Bmatrix} \mathbf{N} \\ \mathbf{M} \end{Bmatrix} = \begin{bmatrix} \mathbf{A} & \mathbf{B} \\ \mathbf{B} & \mathbf{D} \end{bmatrix} \begin{Bmatrix} \boldsymbol{\varepsilon}_m \\ \boldsymbol{\varepsilon}_b \end{Bmatrix} = \mathbf{C}_p \boldsymbol{\varepsilon}_p, \quad (4)$$

$$\mathbf{T} = \begin{bmatrix} k_1^2 \bar{C}_{55}^0 & k_1 k_2 \bar{C}_{45}^0 \\ k_1 k_2 \bar{C}_{45}^0 & k_2^2 \bar{C}_{44}^0 \end{bmatrix} \begin{Bmatrix} \gamma_{xz} \\ \gamma_{yz} \end{Bmatrix} = \mathbf{C}_s \boldsymbol{\gamma}, \quad (5)$$

where $\mathbf{N} = [N_x \quad N_y \quad N_{xy}]^T$, $\mathbf{M} = [M_x \quad M_y \quad M_{xy}]^T$, $\mathbf{T} = [Q_x \quad Q_y]^T$ are the membrane force vector, the bending moment vector and the transverse shear force vector, respectively; k_1^2, k_2^2 are shear correction factors (SCFs) which can be estimated by using special methods [15, 16, 17]; $\mathbf{A}, \mathbf{B}, \mathbf{D}, \mathbf{C}$ are matrices of extensional stiffness, bending-extensional coupling stiffness, bending stiffness and transverse shearing stiffness, respectively defined as

$$\begin{aligned} (A_{ij}, B_{ij}, D_{ij}) &= \int_{-h/2}^{h/2} (1, z, z^2) \bar{Q}_{ij} dz, & i, j &= 1, 2, 6 \\ C_{ij}^0 &= \int_{-h/2}^{h/2} \bar{Q}_{ij} dz, & i, j &= 4, 5 \end{aligned} \quad (6)$$

where \bar{Q}_{ij} are the elastic constants with respect to the global x -axis and their detailed definitions can be found in Ref. [14].

Base on the FSDT, the finite element solution \mathbf{u} of a displacement model for laminated plates is approximated as

$$\mathbf{u} = \begin{Bmatrix} u \\ v \\ w \\ \theta_x \\ \theta_y \end{Bmatrix} = \sum_{i=1}^{np} \begin{bmatrix} N_i & 0 & 0 & 0 & 0 \\ 0 & N_i & 0 & 0 & 0 \\ 0 & 0 & N_i & 0 & 0 \\ 0 & 0 & 0 & N_i & 0 \\ 0 & 0 & 0 & 0 & N_i \end{bmatrix} \mathbf{q}_i, \quad (7)$$

where np ($np = 4$ in this case) is the total number of nodes of an element, $\mathbf{q}_i = [u_i \quad v_i \quad w_i \quad \theta_{xi} \quad \theta_{yi}]^T$ is the nodal displacement vector and $N_i = \frac{1}{4}(1+\xi_i\xi)(1+\eta_i\eta)$ is the shape function of the four-node serendipity element.

The corresponding approximation of membrane, bending and shear strain of Equation (4) can be expressed in the following form

$$\boldsymbol{\varepsilon}_p = \begin{Bmatrix} \boldsymbol{\varepsilon}_m \\ \boldsymbol{\varepsilon}_b \end{Bmatrix} = \begin{bmatrix} \mathbf{B}_m \\ \mathbf{B}_b \end{bmatrix} \mathbf{q} = \mathbf{B}_p \mathbf{q}, \quad (8)$$

$$\boldsymbol{\gamma} = \begin{Bmatrix} \gamma_{xz} \\ \gamma_{yz} \end{Bmatrix} = \mathbf{B}_s \mathbf{q}, \quad (9)$$

$$\mathbf{B}_m = \begin{pmatrix} N_{i,x} & 0 & 0 & 0 & 0 \\ 0 & N_{i,y} & 0 & 0 & 0 \\ N_{i,y} & N_{i,x} & 0 & 0 & 0 \end{pmatrix}, \mathbf{B}_b = \begin{pmatrix} 0 & 0 & 0 & N_{i,x} & 0 \\ 0 & 0 & 0 & 0 & N_{i,y} \\ 0 & 0 & 0 & N_{i,y} & N_{i,x} \end{pmatrix}, \quad (10)$$

$$\mathbf{B}_s = \begin{pmatrix} 0 & 0 & N_{i,x} & N_i & 0 \\ 0 & 0 & N_{i,y} & 0 & N_i \end{pmatrix}. \quad (11)$$

The element stiffness matrix can be written based on the minimum potential principle as

$$\mathbf{K}^e = \mathbf{K}_{mb}^e + \mathbf{K}_s^e = \int_{\Omega^e} \mathbf{B}_p^T \mathbf{C}_p \mathbf{B}_p d\Omega + \int_{\Omega^e} \mathbf{B}_s^T \mathbf{C}_s \mathbf{B}_s d\Omega. \quad (12)$$

By using Hamilton's principle, the equation of motion of an element can be obtained as

$$\mathbf{M}^e \ddot{\mathbf{q}} + \mathbf{K}^e \mathbf{q} = 0, \quad (13)$$

which leads to the following eigenvalue equation

$$(\mathbf{K}^e - \omega^2 \mathbf{M}^e) \mathbf{q} = 0, \quad (14)$$

where the element mass matrix is defined by

$$\mathbf{M}^e = \int_{\Omega^e} \mathbf{N}_m^T \mathbf{m} \mathbf{N}_m d\Omega, \quad (15)$$

in which

$$\mathbf{N}_m = \begin{bmatrix} N_i & 0 & 0 & 0 & 0 \\ 0 & N_i & 0 & 0 & 0 \\ 0 & 0 & N_i & 0 & 0 \\ 0 & 0 & 0 & N_i & 0 \\ 0 & 0 & 0 & 0 & N_i \end{bmatrix}, \mathbf{m} = \rho h \begin{bmatrix} 1 & 0 & 0 & 0 & 0 \\ 0 & 1 & 0 & 0 & 0 \\ 0 & 0 & 1 & 0 & 0 \\ 0 & 0 & 0 & \frac{h^2}{12} & 0 \\ 0 & 0 & 0 & 0 & \frac{h^2}{12} \end{bmatrix}. \quad (16)$$

3 Strain smoothing approach for finite element method

3.1 Smoothed membrane-bending strain approximation

The membrane-bending strains at an arbitrary point \mathbf{x}_C can be obtained by using following strain smoothing operation

$$\tilde{\boldsymbol{\varepsilon}}_p(\mathbf{x}_C) = \int_{\Omega_C} \boldsymbol{\varepsilon}_p(\mathbf{x}) \Phi(\mathbf{x} - \mathbf{x}_C) d\Omega, \quad (17)$$

where $\boldsymbol{\varepsilon}_p$ is the membrane-bending strain obtained from displacement compatibility condition as given in Equation (8); Ω_C is the smoothing cell domain on which the smoothing operation is performed (Ω_C may be an entire element or part of an element as shown in Figure 2, depending on the stability analysis [10, 11]); Φ is a given smoothing function that satisfies at least unity property $\int_{\Omega_C} \Phi d\Omega = 1$ and is defined as

$$\Phi(\mathbf{x} - \mathbf{x}_C) = \begin{cases} 1/A_C & \mathbf{x} \in \Omega_C, \\ 0 & \mathbf{x} \notin \Omega_C, \end{cases} \quad (18)$$

in which $A_C = \int_{\Omega_C} d\Omega$ is the area of the smoothing cell (subcell).

Substituting Φ into Equation (17) and applying the divergence theorem, one can get a smoothed membrane-bending strains as

$$\tilde{\boldsymbol{\varepsilon}}_p(\mathbf{x}_C) = \begin{Bmatrix} \tilde{\boldsymbol{\varepsilon}}_m(\mathbf{x}_C) \\ \tilde{\boldsymbol{\varepsilon}}_b(\mathbf{x}_C) \end{Bmatrix} = \frac{1}{2A_C} \begin{Bmatrix} \int_{\Gamma_C} (u_i n_j + u_j n_i) d\Gamma \\ \int_{\Gamma_C} (\theta_i n_j + \theta_j n_i) d\Gamma \end{Bmatrix}, \quad (19)$$

where Γ_C is the boundary of the smoothing cell.

Introducing the finite element approximation of \mathbf{u} into Equation (7) gives

$$\tilde{\boldsymbol{\varepsilon}}_p(\mathbf{x}_C) = \sum_{i=1}^{nc} [\tilde{\mathbf{B}}_{mi}(\mathbf{x}_C) \tilde{\mathbf{B}}_{bi}(\mathbf{x}_C)]^T \mathbf{q}_i = \sum_{i=1}^{nc} \tilde{\mathbf{B}}_{pi}(\mathbf{x}_C) \mathbf{q}_i, \quad (20)$$

where

$$\tilde{\mathbf{B}}_{pi}(\mathbf{x}_C) = \frac{1}{A_C} \int_{\Gamma_C} \begin{pmatrix} N_i n_x & 0 & 0 & 0 & 0 \\ 0 & N_i n_y & 0 & 0 & 0 \\ N_i n_y & N_i n_x & 0 & 0 & 0 \\ 0 & 0 & 0 & N_i n_x & 0 \\ 0 & 0 & 0 & 0 & N_i n_y \\ 0 & 0 & 0 & N_i n_y & N_i n_x \end{pmatrix} d\Gamma. \quad (21)$$

If one Gaussian point is used to evaluate Equation (21) along each line segment of the boundary Γ_i^C of Ω_C , Equation (21) can be transformed as follows.

$$\tilde{\mathbf{B}}_{pi}(\mathbf{x}_C) = \frac{1}{A_C} \sum_{b=1}^{nb} N_i(\mathbf{x}_b^G) \begin{pmatrix} n_x & 0 & 0 & 0 & 0 \\ 0 & n_y & 0 & 0 & 0 \\ n_y & n_x & 0 & 0 & 0 \\ 0 & 0 & 0 & n_x & 0 \\ 0 & 0 & 0 & 0 & n_y \\ 0 & 0 & 0 & n_y & n_x \end{pmatrix} l_b^C, \quad (22)$$

where x_b^G and l_b^C are the midpoint (Gauss point) and the length of Γ_b^C , respectively; nb is the total number of edges of each smoothing cell.

3.2 Transverse shear strains of the element

The shear strains are approximated with independent interpolation fields in the natural coordinate system [13] as

$$\begin{bmatrix} \gamma_x \\ \gamma_y \end{bmatrix} = \mathbf{J}^{-1} \begin{bmatrix} \gamma_\xi \\ \gamma_\eta \end{bmatrix} = \mathbf{J}^{-1} \hat{\mathbf{N}} \begin{bmatrix} \gamma_\eta^A \\ \gamma_\xi^B \\ \gamma_\eta^C \\ \gamma_\xi^D \end{bmatrix}, \quad (23)$$

in which

$$\hat{\mathbf{N}} = \frac{1}{2} \begin{bmatrix} (1 - \xi) & 0 & (1 + \xi) & 0 \\ 0 & (1 - \eta) & 0 & (1 + \eta) \end{bmatrix}, \quad (24)$$

\mathbf{J} is the Jacobian matrix and the midside nodes A, B, C, D are shown in Figure 1. Expressing $\gamma_\eta^A, \gamma_\eta^C$ and $\gamma_\xi^B, \gamma_\xi^D$ in terms of the discretized fields \mathbf{u} , we obtain the shear matrix

$$\bar{\mathbf{B}}_{si} = \mathbf{J}^{-1} \begin{bmatrix} 0 & 0 & N_{i,\xi} & -b_i^{12} N_{i,\xi} & b_i^{11} N_{i,\xi} \\ 0 & 0 & N_{i,\eta} & -b_i^{22} N_{i,\eta} & b_i^{21} N_{i,\eta} \end{bmatrix}, \quad (25)$$

where

$$b_i^{11} = \xi_i x_{,\xi}^M, \quad b_i^{12} = \xi_i y_{,\xi}^M, \quad b_i^{21} = \eta_i x_{,\eta}^L, \quad b_i^{22} = \eta_i y_{,\eta}^L, \quad (26)$$

in which $\xi_i \in \{-1, 1, 1, -1\}$, $\eta_i \in \{-1, -1, 1, 1\}$
and $(i, M, L) \in \{(1, B, A); (2, B, C); (3, D, C); (4, D, A)\}$.

The element stiffness matrix in Equation (12) can be transformed as follows

$$\tilde{\mathbf{K}}^e = \tilde{\mathbf{K}}_{mb}^e + \bar{\mathbf{K}}_s^e = \sum_{C=1}^{nc} \tilde{\mathbf{B}}_{pC}^T \mathbf{C}_p \tilde{\mathbf{B}}_{pC} A_C + \int_{\Omega_e} \bar{\mathbf{B}}_s^T \mathbf{C}_s \bar{\mathbf{B}}_s d\Omega \quad (27)$$

Finally, the linear equation of motion in Equation (14) can be rewritten as

$$(\tilde{\mathbf{K}}^e - \omega^2 \mathbf{M}^e) \mathbf{q} = 0, \quad (28)$$

In Equation (27), the shear term $\bar{\mathbf{K}}_s^e$ is still computed by 2×2 Gauss quadrature while the element bending stiffness $\tilde{\mathbf{K}}_{mb}^e$ is computed by one Gaussian point along each line segment of the smoothing cells of the element. For simplicity, two smoothing cells ($nc = 2$) as shown in Figure 2 are used

for calculating the smoothed membrane-bending stiffness matrix of the element. This forms the basis of a new four-node quadrilateral element named MISQ20 (Mixed Interpolation Smoothing Quadrilateral element with 20 DOF) for analysis of laminated plates. For analysis of laminated shells using MISQ20 flat element, a drilling degree of freedom θ_z (inplane rotation) will be added to each node for assembling the stiffness matrices and the total DOFs will be 24. To avoid rank deficiency of the element stiffness matrix, the fictitious stiffness associated with the drilling DOF is taken to be equal to 1/1000 of the maximum diagonal value of the element stiffness matrix.

4 Numerical results and discussions

In this section, a number of numerical examples are presented to demonstrate the performance of the MISQ20 element in the analysis of free vibration of laminated plates/shells. Particular plate/shell structures with various boundary conditions, span-to-thickness ratios and modulus ratios (the degree of orthotropy) are analyzed. In all examples, the material properties are assumed to be the same in all the layers and the fibre orientations may be different among the layers. The ply angle of each layer is measured from the global x -axis to the fibre direction. All layers have the same thickness and the mass density ρ is taken to be uniform in the thickness direction. Unless otherwise specified, shear correction factors $k_1^2 = k_2^2 = \frac{\pi^2}{12}$ are used for all computations. The following material parameters of a layer are used in all plate examples $E_1/E_2 = 10, 20, 30$ or 40 ; $G_{12} = G_{13} = 0.6E_2$; $G_{23} = 0.5E_2$; $\nu_{12} = \nu_{13} = \nu_{23} = 0.25$; $\rho = 1$.

4.1 Square laminated plates

This section deals with cross-ply laminated square plates with various span-to-thickness ratios, number of layers, boundary conditions and lay-up stacking sequences. A typical representative sketch of a mesh of 14×14 used in these analyses is shown in Figure 3.

4.1.1 Convergence study and the effect of modulus ratios

A simply supported four-layer cross-ply $[0/90/90/0]$ square laminated plate is chosen to study the convergence of the present method using MISQ20 element. The span-to-thickness ratio of the plate a/h is taken to be 5 in the computation. Table 1 shows the convergence and comparison of the normalized fundamental frequencies of the present method with other solutions for

various degrees of orthotropy of the individual layers (E_1/E_2 ratio). It is found that the MISQ20 element yields not only relatively accurate results in a wide range of E_1 to E_2 ratios but also rapid convergence as shown in Figure 4a. The effect of various modulus ratios of E_1/E_2 on the accuracy of the fundamental frequency is also displayed in Figure 4b. It can be seen that the present results are in good agreement with exact solutions [14, 18] and closer to MLSDQ's solutions by Liew *et al.* [5] than RBF's results of Ferreira *et al.* [7].

4.1.2 Mesh distortion

The influence of mesh distortion is studied in this section. The plate of the first example (Section 4.1.1) is analyzed again using distorted element created by irregular interior nodes. These interior nodes are derived from a set of regular nodes by using a controlling distortion factor s . Thus, the coordinates of an irregular mesh are obtained by the following expressions

$$\begin{aligned}x' &= x + r_c s \Delta x, \\y' &= y + r_c s \Delta y,\end{aligned}\tag{29}$$

where r_c is a computer-generated random number between -1.0 and 1.0 , $\Delta x, \Delta y$ are initial regular element sizes in the x - and y -directions, respectively and $s \in [0, 0.4]$ is used to control the shapes of the distorted elements: the bigger value of s , the more irregular the shape of generated elements. Typical irregular meshes of the analysis are shown in Figure 5.

The effect of the mesh distortion on the fundamental frequency of the plate obtained by the present method is shown in Table 2 and Figure 6. It is found that the accuracy of the fundamental frequencies associated with irregular mesh decreases in comparison with regular meshes. However, the deterioration is very small and the overall performance is insensitive to mesh distortion as the maximum error of frequency is below 0.3% (in the case of $E_1/E_2 = 10$). For the cases of $E_1/E_2 = 30$ and 40, Figure 6 indicates that the error at some s could become even smaller than those at $s = 0$ (regular mesh).

4.1.3 Effect of span-to-thickness ratio

This section deals with the effect of the span-to-thickness ratio (a/h) on the fundamental frequency of a simply supported square cross-ply plate made of material having $E_1/E_2 = 40$. Table 3 presents a convergence study on the normalized fundamental frequency. The present numerical results are comparable with those of Reddy and Phan [19] who used higher-order shear deformation theory, Liew [20] who used a p-Ritz solution, Wu *et al.* [21] who used local higher-order theory, Matsunaga [22] who used global higher-order theory, Striz

et al. [23] who used higher-order individual-layer theory and Zhen *et al.* [24] who used global-local higher-order theory. However, it can be seen that the present results are in closer agreement with results of Liew than other methods cited here. From Table 3, it is also noticed that the span-to-thickness ratio has a considerable effect on the fundamental frequency of plates at lower a/h ratios. At higher a/h ratios ($a/h > 25$), the influence on the fundamental frequency is minor.

4.1.4 Effect of lay-up sequence and fibre orientation

To investigate the effect of lay-up sequence and fibre orientation, this section reports the analysis of two composite plates with lamination sequence $[\theta/0/0/\theta]$ and $[0/\theta/\theta/0]$ with simply supported (SSSS) and clamped (CCCC) edges. The span-to-thickness ratio of the plate $a/h = 100$ and modulus ratio $E_1/E_2 = 10$ are used in the computation. Figure 7 shows the effects of both fibre orientation and lay-up sequence on the fundamental frequencies. It is found that there is symmetry for the orientation angle of 45 degrees in both cases of simply supported and clamped conditions. Moreover, in the case of SSSS edge conditions, the $[\theta/0/0/\theta]$ lamination results in a higher fundamental frequencies than the corresponding ones for the $[0/\theta/\theta/0]$ sequence. In the case of CCCC edge conditions, the behaviour of the fundamental frequencies is opposite to the above SSSS results. It appears that, in both cases, the fundamental frequencies has an extremum at ply angle $\theta = 45^\circ$.

4.1.5 Influence of mixed boundaries and span-to-thickness ratio

The influence of the mixed boundary conditions and span-to-thickness ratio is now considered. The plate is simply supported along the edges parallel to the x -axis while the other edges have simply supported (S), clamped (C) or free (F) boundary conditions. The notation SS, SC, CC, FF, FS and FC refer to the boundary conditions of two edges parallel to the y -axis only. The three layer cross-ply $[0/90/0]$ square plate is analyzed with $E_1 = 40E_2$ and a 14×14 mesh as indicated in Figure 3. Table 4 contains the normalized fundamental frequencies for various span-to-thickness ratios obtained by the present method and other solutions of Liew *et al.*[5] using MLSDQ method, RBF's results by Ferreira *et al.* [7] and exact solutions [14, 18]. It can be seen that the accuracy of the present method compares very well with exact solutions and other numerical results.

Furthermore, the comparison of the first five natural frequencies with other methods for a clamped 3-layer cross-ply $[0/90/0]$ square plate is also presented in Table 5. The first four mode shapes obtained by the present method are also depicted on Figure 8. It is found that the present results in general indicate

good agreement with other cited solutions.

4.2 Skew laminated plates

This section deals with five-layer symmetric cross-ply and angle-ply skew laminated plates. Simply supported and clamped edges are considered with various skew angles α from 0° to 60° . The span-to-thickness ratio a/h is taken to be 10 and the entire plate is modelled using 6×6 , 10×10 and 14×14 meshes. A representative sketch of the 10×10 mesh used in the analysis is displayed in Figure 9.

Table 6 and Table 7 present the normalized fundamental frequencies of the cross-ply $[90/0/90/0/90]$ with simply supported and clamped edges, respectively while Table 8 and Table 9 show the normalized fundamental frequencies of the angle-ply $[45/-45/45/-45/45]$ with simply supported and clamped boundaries. The results calculated using MLSDQ method by Liew *et al.* [5], B-spline Rayleigh-Ritz method of Wang *et al.* [26] and RBF of Ferreira *et al.* [7] are also listed for comparison. It can be seen that there is a good agreement between the present results and other existing solutions for both cases of cross-ply and angle-ply laminates. The numerical accuracy is slightly dependent on the skew angle α (accuracy deteriorates with increasing α) but insensitive to lay-up sequence. The first four mode shapes obtained by the present methods for CCCC and SSSS cases of the $[90/0/90/0/90]$ laminated plates are also depicted in Figure 10 and Figure 11, respectively.

4.3 Circular laminated plates

A circular symmetric 4-layer $[\theta/-\theta/-\theta/\theta]$ laminated plate with a diameter D and a thickness h as shown in Figure 12 is analysed. The span-to-thickness ratio a/h is taken to be 10 in the computation. Two types of boundary conditions, simply supported (SSSS) and clamped (CCCC) with various fibre orientation angles $\theta = 0^\circ, 15^\circ, 30^\circ, 45^\circ$ are considered.

The effect of the ply angle θ on the normalized fundamental frequency of the simply supported and clamped circular laminated plate is presented in Table 10. The natural frequencies of the first six modes in the case of clamped edge conditions are also presented in Table 11. It is observed that the numerical results obtained by the present method are comparable with Liew's results [5].

4.4 Multi-layer cylindrical shells

The cross-ply laminated cylindrical panel with a radius $R = 100$ and a side length $L = 20$ subjected to simply supported boundaries is studied. The total thickness of the panel is $h = 0.2$. All layers have equal thickness and are made of the same material: $E_1/E_2 = 25, G_{12} = G_{13} = 0.5E_2, G_{23} = 0.2E_2, \nu_{12} = \nu_{13} = \nu_{23} = 0.25, \rho = 1$. The SCFs are assumed to be $5/6$. Three kinds of lay-up sequence: $[0/90], [0/90/0]$ and $[0/90/90/0]$ are considered. Considering only doubly symmetric modes, a quadrant designated as ABCD as shown in Figure 13 is modeled. The $4 \times 4, 6 \times 6$ and 8×8 meshes are used in computing the fundamental frequencies associated with the doubly symmetric modes. The convergence study of the normalized fundamental frequency is presented in Table 12. The present results are also compared with other numerical solutions such as results of Liu and To using layer-wise shell element [27], of Jayasankar using 9-node degenerated shell element [28] and the analytical solution by Reddy [29].

It can be seen that the accuracy of the present element is compared very favorably with other elements and the method is also convergent with mesh refinement. The present element can provide accurate prediction of the solution with much reduced degrees of freedom and its performance with respect to analytical solution is excellent.

4.5 Multi-layer spherical shell

A clamped nine-layered cross-ply $[0/90/0/90/0/90/0/90/0]$ laminated spherical panel as shown in Figure 14 is considered. The panel has a radius $R = 10$ and a side length $a = 1$. The total thickness of the panel is $h = 0.01$. All layers are of equal thickness and same material properties: $E_1 = 2.0685 \times 10^{11}, E_2 = E_1/40, G_{12} = G_{13} = 0.5E_2, G_{23} = 0.6E_2, \nu_{12} = 0.25$ and $\rho = 1605$. The SCFs are $k_1^2 = k_2^2 = 5/6$. Three different finite element meshes are used $6 \times 6, 10 \times 10$, and 14×14 for modelling a full sphere shell.

Table 13 gives the first four normalized natural frequencies obtained by the present method in comparison with the solution of Jayasankar [28] using nine-node degenerated shell element. It can be seen that the present results agree well with the solutions given by Jayasankar.

5 Conclusions

In this paper, the MISQ20 element is further developed and successfully applied to analyse the free vibration of laminated plate/shell structures within the framework of the first-order shear deformation plate theory (FSDT). Several numerical investigations are conducted and the obtained results are in excellent agreement with other available numerical and analytic solutions. It is found that the present element is relatively simple but yields slightly better accuracy for thin to thick laminated plates/shells with various boundary conditions, modulus ratios and stacking sequences. Since the integration is done on the element boundaries for the bending and membrane terms, the present element remains accurate even when it is highly distorted.

6 Acknowledgements

The first author is supported by the Faculty of Engineering and Surveying (FoES) and the Computational Engineering & Science Research Centre (CESRC), USQ, Australia. These supports are gratefully acknowledged. We also would like to thank the referees for their helpful comments.

References

- [1] Bert CW. Research on dynamics of composite sandwich plates. *Shock and Vibration Digest* 1982; 14:17–34.
- [2] Mohamad SQ. Recent research advances in the dynamic behavior of shell: 1989–2000, Part 1: Laminated composite shells. *ASME Applied Mechanics Reviews* 2002; 55(4):325–350
- [3] Yang HTY, Saigal S, Masud A, Kapania RK. A survey of recent shell finite elements. *International Journal for Numerical Methods in Engineering* 2000; 47:101–127.
- [4] Lim SP, Chen XL, Liu GR. An element free Galerkin method for the free vibration analysis of composite laminates of complicated shape. *Composite Structures* 2003; 59:279–289.
- [5] Liew KM, Huang YQ, Reddy JN. Vibration analysis of symmetrically laminated plates based on FSDT using the moving least squares differential quadrature method. *Computer Methods in Applied Mechanics and Engineering* 2003; 192:2203–2222.
- [6] Lanhe W, Hua L, Daobin W. Vibration analysis of generally laminated composite plates by the moving least squares differential quadrature method. *Composite Structures* 2005; 68:319–330.

- [7] Ferreira AJM, Jorge RMN, Roque CMC. Free vibration analysis of symmetric laminated composite plates by FSDT and radial basis functions. *Computer Methods in Applied Mechanics and Engineering* 2005; 194:4265–4278.
- [8] Ferreira AJM, Fasshauer GE. Analysis of natural frequencies of composite plates by an RBF-pseudospectral method. *Composite Structures* 2007; 79(2):202–210.
- [9] Wang J, Liew KM, Tan MJ, Rajendran S. Analysis of rectangular laminated composite plates via FSDT meshless method. *International Journal of Mechanical Sciences* 2002; 44:1275–1293.
- [10] Liu GR, Dai KY, Nguyen TT. A smoothed finite element method for mechanics problems. *Computational Mechanics* 2007; 39(6):859–877.
- [11] Liu GR, Nguyen TT, Dai KY, Lam KY. Theoretical aspects of the smoothed finite element method (SFEM). *International Journal for Numerical Methods in Engineering* 2006; 71(8): 902–930
- [12] Nguyen-Van H, Mai-Duy N, Tran-Cong T. A simple and accurate four-node quadrilateral element using stabilized nodal integration for laminated plates. *CMC: Computers, Materials & Continua* 2007; 6(3): 159–175.
- [13] Dvorkin EN, Bathe KJ. A four node plate bending element based on Mindlin-Reissner plate theory and a mixed interpolation. *International Journal for Numerical Methods in Engineering* 1985; 21:367–383.
- [14] Reddy JN. *Mechanics of laminated composite plates and shells-Theory and analysis*. CRC Press, 2004.
- [15] Valchoutsis S. Shear correction factors for plates and shells. *International Journal for Numerical Methods in Engineering* 1992; 33:1537–1552.
- [16] Kulkarni SV, Chatterjee SN. Shear correction factors for laminated plates. *AIAA Journal* 1979; 17:498–499.
- [17] Whitney JM. Shear correction factors for orthotropic laminates under static load. *Journal of Applied Mechanics* 1973; 40:302–304.
- [18] Khdeir AA, Librescu L. Analysis of symmetric cross-ply elastic plates using a higher-order theory. Part II: buckling and free vibration. *Composite Structures* 1988; 9:259–277.
- [19] Reddy JN, Phan PH. Stability and vibration of isotropic, orthotropic and laminated plates according to a higher order shear deformation theory. *Journal of Sound and Vibration* 1985; 98:157–170.
- [20] Liew KM. Solving the vibration of thick symmetric laminates by Reissner/Mindlin plate theory and the p-Ritz method. *Journal of Sound and Vibration* 1996; 198(3):343–360.
- [21] Wu CP, Chen WY. Vibration and stability of laminated plates based on a local higher-order plate theory. *Journal of Sound and Vibration* 1994; 177(4):503–520.
- [22] Matsunaga H. Vibration and stability of cross-ply laminated composite plates according to a global higher-order plate theory. *Composite Structures* 2000; 48:231–244.

- [23] Striz AG, Cho KN, Bert CW. Free vibration of laminated rectangular plates analyzed by higher-order individual-layer theory. *Journal of Sound and Vibration* 1991; 145:429–442.
- [24] Zhen W, Wanji C. Free vibration of laminated composite and sandwich plates using global-local higher-order theory. *Journal of Sound and Vibration* 2006; 298:333–349.
- [25] Jian WS, Akihiro N, Hiroshi K. Vibration analysis of fully clamped arbitrary laminated plate. *Composite Structures* 2004; 63:115–122.
- [26] Wang S. Free vibration analysis of skew fibre-reinforced composite laminates based on first-order shear deformation plate theory. *Computer & Structures* 1997; 63:525–538.
- [27] Liu ML, To CWS. Free vibration analysis of laminated composite shell structures using hybrid strain based layerwise finite elements. *Finite Elements in Analysis and Design* 2003; 40:83-120.
- [28] Jayasankar S, Mahesh S, Narayanan S, Padmanabhan C. Dynamic analysis of layered composite shells using nine node degenerate shell elements. *Journal of Sound and Vibration* 2007; 299:1–11.
- [29] Reddy JN. Exact solutions of moderately thick laminated shells. *ASCE Journal of Engineering Mechanics* 1984; 110(4):794–809.

Table 1

Simply supported cross-ply [0/90/90/0] square plate: Convergence of normalized fundamental frequencies and comparison with other solutions ($\omega^* = (\omega a^2/h)\sqrt{\rho/E_2}$, $a/h = 5$).

| Model | Mesh | E_1/E_2 | | | |
|----------------|-------|-----------|--------|---------|---------|
| | | 10 | 20 | 30 | 40 |
| MISQ20 | 6×6 | 8.4443 | 9.7149 | 10.4729 | 11.0001 |
| | 10×10 | 8.3384 | 9.6010 | 10.3548 | 10.8792 |
| | 12×12 | 8.3203 | 9.5815 | 10.3346 | 10.8585 |
| | 14×14 | 8.3094 | 9.5698 | 10.3224 | 10.8471 |
| MLSDQ [5] | | 8.2924 | 9.5613 | 10.320 | 10.849 |
| RBF [7] | | 8.3101 | 9.5801 | 10.349 | 10.864 |
| Exact [18, 14] | | 8.2982 | 9.5671 | 10.326 | 10.854 |

Table 2

Simply supported cross-ply [0/90/90/0] square plate: Effect of mesh distortion on the normalized fundamental frequencies ($\omega^* = (\omega a^2/h)\sqrt{\rho/E_2}$, $a/h = 5$).

| E_1/E_2 | $s = 0$ | $s = 0.1$ | $s = 0.2$ | $s = 0.3$ | $s = 0.4$ |
|-----------|---------|-----------|-----------|-----------|-----------|
| 40 | 10.8471 | 10.8476 | 10.8495 | 10.8528 | 10.8597 |
| 30 | 10.3224 | 10.3239 | 10.3257 | 10.3283 | 10.3354 |
| 20 | 9.5698 | 9.5712 | 9.5728 | 9.5749 | 9.5820 |
| 10 | 8.3094 | 8.3108 | 8.3125 | 8.3140 | 8.3207 |

Table 3

Simply supported cross-ply [0/90/90/0] square plate with various a/h ratios: Convergence of normalized fundamental frequencies and comparison with other solutions ($\omega^* = (\omega a^2/h)\sqrt{\rho/E_2}$, $E_1/E_2 = 40$).

| Model | a/h | | | | | | |
|--------------------------|-------|---------|---------|---------|---------|---------|---------|
| | 5 | 10 | 20 | 25 | 50 | 100 | |
| | 6×6 | 11.0001 | 15.4187 | 18.0504 | 18.4839 | 19.1221 | 19.2939 |
| MISQ20 | 10×10 | 10.8792 | 15.2201 | 17.7903 | 18.2122 | 18.8325 | 18.9992 |
| | 14×14 | 10.8461 | 15.1658 | 17.7192 | 18.1380 | 18.7535 | 18.9189 |
| p-Ritz [20] | | 10.8550 | 15.1434 | 17.6583 | 18.0718 | 18.6734 | 18.8359 |
| RBF-pseudospectral [8] | | 10.8074 | 15.1007 | 17.6338 | 18.0490 | 18.6586 | 18.8223 |
| Reddy & Phan [19] | | 10.9891 | 15.2689 | 17.6669 | 18.0490 | 18.4624 | 18.7561 |
| Cho <i>et al.</i> [23] | | 10.673 | 15.066 | 17.535 | 18.054 | 18.670 | 18.835 |
| Local theory[21] | | 10.682 | 15.069 | 17.636 | 18.055 | 18.670 | 18.835 |
| Global theory [22] | | 10.6876 | 15.0721 | 17.6369 | 18.0557 | 18.6702 | 18.8352 |
| Global-local theory [24] | | 10.7294 | 15.1658 | 17.8035 | 18.2404 | 18.9022 | 19.1566 |

Table 4

Cross-ply [0/90/0] square plate with various mixed boundaries and span-to-thickness ratios: Comparison of normalized fundamental frequencies with other solutions ($\omega^* = (\omega a^2/h)\sqrt{\rho/E_2}$, $E_1/E_2 = 40$).

| a/h | Model | SS | SC | CC | FF | FS | FC |
|-------|---------------|----------------------|----------------------|----------------------|--------------------|--------------------|---------------------|
| 5 | MISQ20 | 10.2780 (-0.117%) | 10.6280 (-0.169%) | 11.2387 (-0.242%) | 4.0717 (0.461%) | 4.5613 (0.381%) | 5.9370 (0%) |
| | RBF [7] | 10.307 (0.165%) | 10.658 (0.113%) | 11.274 (0.071%) | – | – | – |
| | MLSDQ [5] | 10.290 (0%) | 10.647 (0.009%) | 11.266 (0%) | 4.054 (0.025%) | 4.545 (0.022%) | 5.938 (0.017%) |
| | Exact[18, 14] | 10.290 | 10.646 | 11.266 | 4.053 | 4.544 | 5.937 |
| 10 | MISQ20 | 14.7823 (0.110%) | 17.1806 (0.033%) | 19.6614 (-0.039%) | 4.3679 (0.573%) | 4.9401 (0.531%) | 7.3372 (0.084%) |
| | RBF [7] | 14.804 (0.257%) | 17.199 (0.139%) | 19.678 (0.046%) | – | – | – |
| | MLSDQ [5] | 14.767 (0.007%) | 17.176 (0.006%) | 19.669 (0%) | 4.343 (0%) | 4.917 (0.061%) | 7.333 (0.028%) |
| | Exact[18, 14] | 14.766 | 17.175 | 19.669 | 4.343 | 4.914 | 7.331 |
| 100 | MISQ20 | 18.9095 (0.098%) | 28.4750 (-0.091%) | 40.5937 (-0.366%) | 4.4835 (0.594%) | 5.1007 (0.487%) | 8.2665 (-0.030%) |
| | RBF [7] | 18.355 (-2.837%) | 28.165 (-1.179%) | 40.234 (-1.249%) | – | – | – |
| | MLSDQ [5] | 18.769 (-0.646%) | 28.164 (-1.182%) | 40.004 (-1.814%) | 4.439 (-0.404%) | 5.301 (4.433%) | 8.451 (2.201%) |
| | Exact[18, 14] | 18.891 | 28.501 | 40.743 | 4.457 | 5.076 | 8.269 |

The values in parentheses correspond to relative error percentage when compared to exact solution

Table 5

Clamped cross-ply [0/90/0] square plate: Comparison of the first five natural frequencies with other solutions.

| a/h | Model | Mode | | | | |
|-------|-------------------------|---------|---------|---------|---------|---------|
| | | 1 | 2 | 3 | 4 | 5 |
| 5 | MISQ20 | 4.4671 | 6.7365 | 7.7706 | 8.7678 | 9.2988 |
| | p-Ritz [20] | 4.447 | 6.642 | 7.700 | 9.185 | 9.738 |
| | Global-local[24] | 4.540 | 6.524 | 8.178 | 9.473 | 9.492 |
| 10 | MISQ20 | 7.4542 | 10.5909 | 14.0808 | 16.0497 | 16.0868 |
| | p-Ritz [20] | 7.411 | 10.393 | 13.913 | 15.429 | 15.806 |
| | MLSDQ [6] | 7.432 | 10.399 | 13.958 | 15.467 | 15.838 |
| | Global-local[24] | 7.484 | 10.207 | 14.340 | 14.863 | 16.070 |
| | Jian <i>et al.</i> [25] | 7.451 | 10.451 | 13.993 | 15.534 | 15.896 |
| 20 | MISQ20 | 11.0454 | 14.2988 | 21.4609 | 23.6389 | 25.4605 |
| | p-Ritz [20] | 10.953 | 14.028 | 20.388 | 23.196 | 24.978 |
| | Global-local[24] | 11.003 | 14.064 | 20.321 | 23.498 | 25.350 |
| | Jian <i>et al.</i> [25] | 11.015 | 14.152 | 20.691 | 23.323 | 25.142 |
| 100 | MISQ20 | 14.6199 | 17.7013 | 25.5625 | 38.2411 | 39.3269 |
| | p-Ritz [20] | 14.666 | 17.614 | 24.511 | 35.532 | 39.157 |
| | MLSDQ [6] | 14.674 | 17.668 | 24.594 | 35.897 | 39.625 |
| | Global-local[24] | 14.601 | 17.812 | 25.236 | 37.168 | 38.528 |
| | Jian <i>et al.</i> [25] | 14.583 | 17.762 | 25.004 | 36.644 | 38.073 |

Table 6

Simply supported cross-ply [90/0/90/0/90] skew plate with various skew angles: Convergence of fundamental frequencies and comparison with other solutions ($\omega^* = (\omega a^2 \sqrt{\rho/E_2})/(\pi^2 h)$, $E_1/E_2 = 40$, $a/h = 10$).

| Model | Mesh | α | | | | |
|--------------|----------------|----------|--------|--------|--------|--------|
| | | 0^0 | 15^0 | 30^0 | 45^0 | 60^0 |
| MISQ20 | 6×6 | 1.6030 | 1.7267 | 2.1441 | 3.0021 | 4.7710 |
| | 10×10 | 1.5797 | 1.6977 | 2.0963 | 2.9141 | 4.6033 |
| | 14×14 | 1.5733 | 1.6896 | 2.0820 | 2.8855 | 4.5412 |
| MLSDQ [5] | | 1.5709 | 1.6886 | 2.1026 | 2.8798 | 4.4998 |
| RBF [7] | | 1.5791 | 1.6917 | 2.0799 | 2.8228 | 4.3761 |
| B-spline[26] | | 1.5699 | – | 2.0844 | 2.8825 | – |

Table 7

Clamped cross-ply [90/0/90/0/90] skew plate with various skew angles: Convergence of fundamental frequencies and comparison with other solutions ($\omega^* = (\omega a^2 \sqrt{\rho/E_2})/(\pi^2 h)$, $E_1/E_2 = 40$, $a/h = 10$).

| Model | Mesh | α | | | | |
|--------------|----------------|----------|--------|--------|--------|--------|
| | | 0^0 | 15^0 | 30^0 | 45^0 | 60^0 |
| MISQ20 | 6×6 | 2.4550 | 2.5528 | 2.8901 | 3.6260 | 5.2538 |
| | 10×10 | 2.4014 | 2.4958 | 2.8194 | 3.5200 | 5.0610 |
| | 14×14 | 2.3869 | 2.4803 | 2.7998 | 3.4893 | 4.9989 |
| MLSDQ [5] | | 2.3790 | 2.4725 | 2.7927 | 3.4723 | 4.9430 |
| RBF [7] | | 2.4021 | 2.4932 | 2.8005 | 3.4923 | 4.9541 |
| B-spline[26] | | 2.3820 | – | 2.7921 | 3.4738 | – |

Table 8

Simply supported angle-ply [45/-45/45/-45/45] skew plate with various skew angles: Convergence of fundamental frequencies and comparison with other solutions ($\omega^* = (\omega a^2 \sqrt{\rho/E_2})/(\pi^2 h)$, $E_1/E_2 = 40$, $a/h = 10$).

| Model | Mesh | α | | | | |
|--------------|----------------|----------|--------|--------|--------|--------|
| | | 0^0 | 15^0 | 30^0 | 45^0 | 60^0 |
| MISQ20 | 6×6 | 1.8768 | 1.9255 | 2.1546 | 2.7185 | 4.1758 |
| | 10×10 | 1.8491 | 1.8969 | 2.1093 | 2.6286 | 4.0249 |
| | 14×14 | 1.8413 | 1.8889 | 2.0955 | 2.5672 | 3.9718 |
| MLSDQ [5] | | 1.8248 | 1.8838 | 2.0074 | 2.5028 | 4.0227 |
| RBF [7] | | 1.8357 | 1.8586 | 2.0382 | 2.4862 | 3.8619 |
| B-spline[26] | | 1.8792 | – | 2.0002 | 2.4788 | – |

Table 9

Clamped angle-ply [45/-45/45/-45/45] skew plate with various skew angles: Convergence of fundamental frequencies and comparison with other solutions ($\omega^* = (\omega a^2 \sqrt{\rho/E_2})/(\pi^2 h)$, $E_1/E_2 = 40$, $a/h = 10$).

| Model | Mesh | α | | | | |
|--------------|----------------|----------|--------|--------|--------|--------|
| | | 0^0 | 15^0 | 30^0 | 45^0 | 60^0 |
| MISQ20 | 6×6 | 2.3551 | 2.4242 | 2.7566 | 3.5013 | 5.1549 |
| | 10×10 | 2.3045 | 2.3713 | 2.6892 | 3.3977 | 4.9605 |
| | 14×14 | 2.2908 | 2.3570 | 2.6708 | 3.3683 | 4.8982 |
| MLSDQ [5] | | 2.2787 | 2.3504 | 2.6636 | 3.3594 | 4.8566 |
| RBF [7] | | 2.3324 | 2.3962 | 2.6981 | 3.3747 | 4.8548 |
| B-spline[26] | | 2.2857 | – | 2.6626 | 3.3523 | – |

Table 10

Circular 4-layer $[\theta/ - \theta/ - \theta/\theta]$ laminated plates with various boundary conditions and ply angles: Comparison of fundamental frequencies with other solutions ($\omega^* = (\omega a^2/h)\sqrt{\rho/E_2}$, $E_1/E_2 = 40$, $a/h = 10$).

| Model | B.C | θ | | | |
|-----------|------|----------|--------|--------|--------|
| | | 0 | 15 | 30 | 45 |
| MISQ20 | SSSS | 16.168 | 16.448 | 16.924 | 17.162 |
| MLSDQ [5] | | 16.167 | 16.475 | 16.928 | 17.119 |
| MISQ20 | CCCC | 22.123 | 22.698 | 24.046 | 24.766 |
| MLSDQ [5] | | 22.211 | 22.774 | 24.071 | 24.752 |

Table 11

Clamped circular 4-layer $[\theta/ - \theta/ - \theta/\theta]$ laminated plate: Comparison of the normalized natural frequencies of the first six modes ($\omega^* = (\omega a^2/h)\sqrt{\rho/E_2}$, $E_1/E_2 = 40$, $a/h = 10$).

| θ | Model | Mode | | | | | |
|----------|-----------|--------|--------|--------|--------|--------|--------|
| | | 1 | 2 | 3 | 4 | 5 | 6 |
| 0 | MISQ20 | 22.123 | 29.768 | 41.726 | 42.805 | 50.756 | 56.950 |
| | MLSDQ [5] | 22.211 | 29.651 | 41.101 | 42.635 | 50.309 | 54.553 |
| 15 | MISQ20 | 22.698 | 31.568 | 43.635 | 44.318 | 53.468 | 60.012 |
| | MLSDQ [5] | 22.774 | 31.455 | 43.350 | 43.469 | 52.872 | 57.386 |
| 30 | MISQ20 | 24.046 | 36.399 | 44.189 | 52.028 | 57.478 | 67.099 |
| | MLSDQ [5] | 24.071 | 36.153 | 43.968 | 51.074 | 56.315 | 66.220 |
| 45 | MISQ20 | 24.766 | 39.441 | 43.817 | 57.907 | 57.945 | 66.297 |
| | MLSDQ [5] | 24.752 | 39.181 | 43.607 | 56.759 | 56.967 | 65.571 |

Table 12

Simply supported laminated cylindrical shells: Convergence of normalized fundamental frequencies $\omega^* = (\omega L^2/h)\sqrt{\rho/E_2}$ for doubly symmetric modes and comparison with other solutions.

| Model | Mesh | Lay-up | | |
|-------------------|--------------|----------|-----------|-------------|
| | | [0/90] | [0/90/0] | [0/90/90/0] |
| MISQ20 | 4×4 | 17.061 | 20.575 | 20.694 |
| | 6×6 | 16.833 | 20.340 | 20.461 |
| | 8×8 | 16.736 | 20.240 | 20.367 |
| | | (0.408%) | (-0.452%) | (0.029%) |
| Layer-wise [27] | 8×8 | 17.390 | 20.960 | 20.960 |
| | | (4.332%) | (3.089%) | (2.942%) |
| 9-node shell [28] | 5×5 | 17.7 | - | - |
| | | (6.192%) | - | - |
| Analytic [29] | | 16.668 | 20.332 | 20.361 |

Table 13

Clamped 9-layer $[(0/90)_2/0_s]$ cross-ply spherical shell: Comparison the normalized fundamental frequencies $\omega^* = (\omega a^2/h)\sqrt{\rho/E_2}$ with other solutions.

| Model | Mesh | Mode 1 | Mode 2 | Mode 3 | Mode 4 |
|-------------------|----------------|--------|--------|--------|--------|
| MISQ20 | 6×6 | 69.61 | 98.25 | 118.15 | 136.05 |
| | 10×10 | 67.94 | 88.24 | 104.45 | 119.73 |
| | 14×14 | 67.51 | 86.00 | 101.27 | 115.88 |
| 9-node shell [28] | 15×15 | 67.43 | 84.16 | 99.71 | 113.70 |

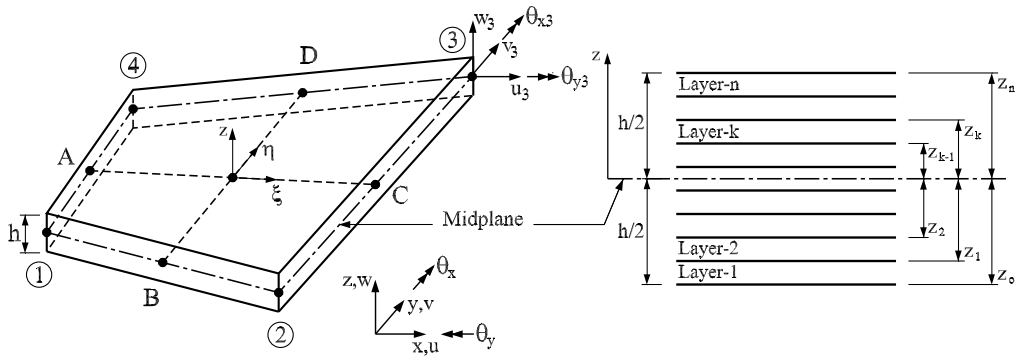


Fig. 1. A quadrilateral laminated plate element consisting of n layers

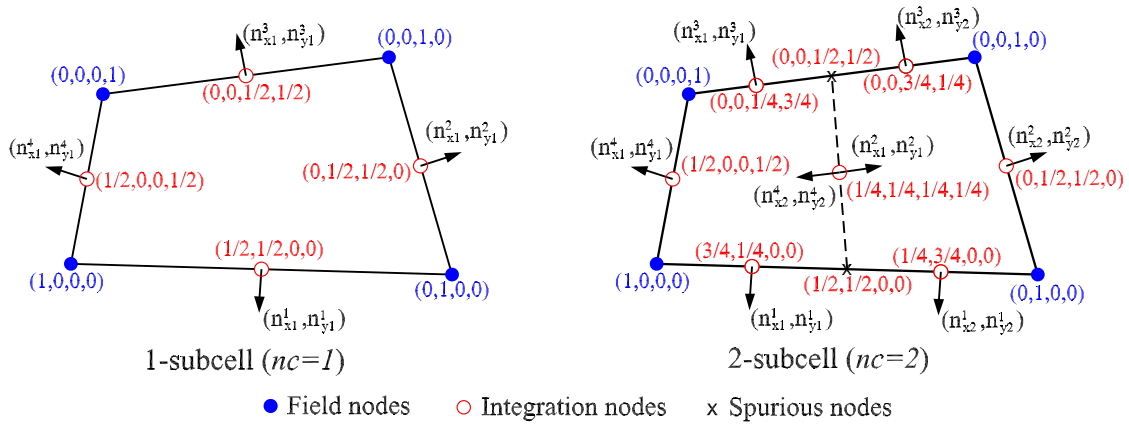


Fig. 2. Subdivision of an element into smoothing cells (nc) and the values of shape functions at nodes.

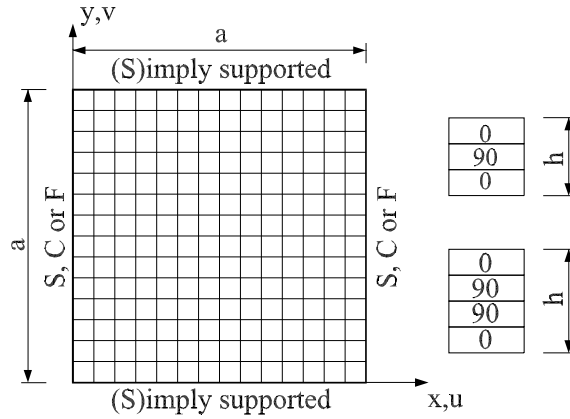
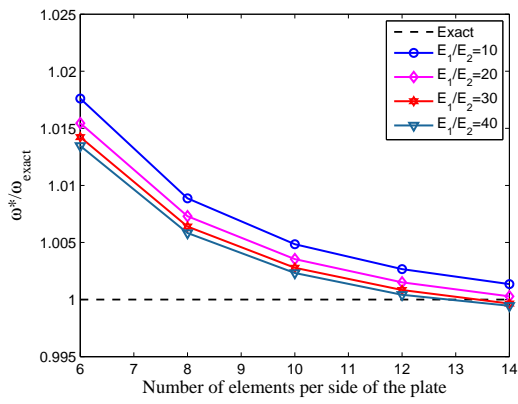
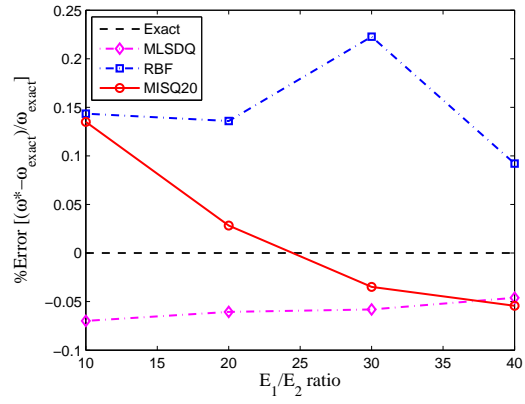


Fig. 3. Geometry and discretization of square laminated plates



(a) Convergence study



(b) Effect of modulus ratios

Fig. 4. Square cross-ply $[0/90/90/0]$ laminated plate: Convergence of the present method and effect of modulus ratios on the accuracy of fundamental frequencies.

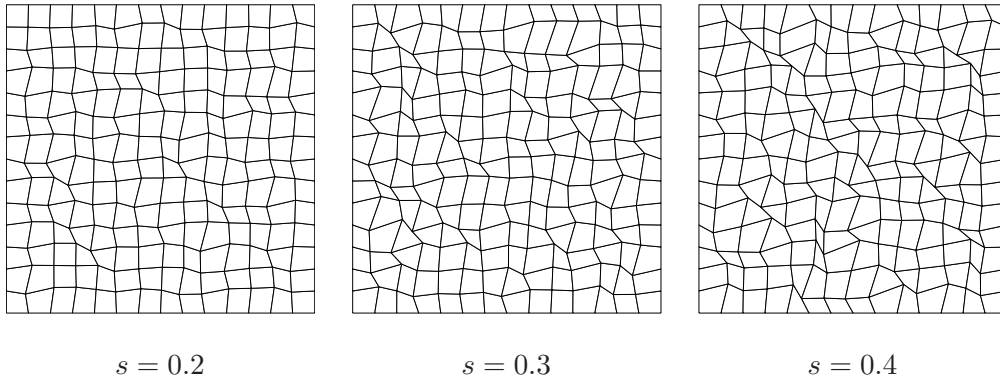


Fig. 5. Typical irregular meshes with various distortion factor s .

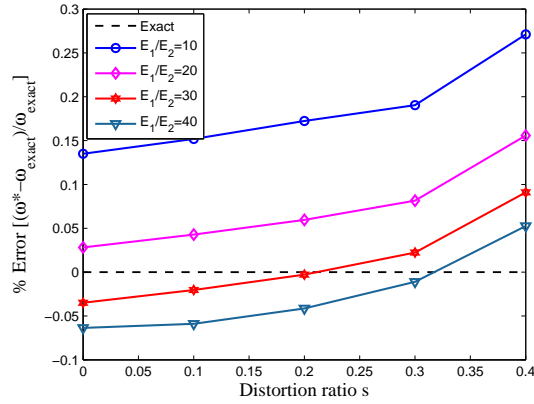
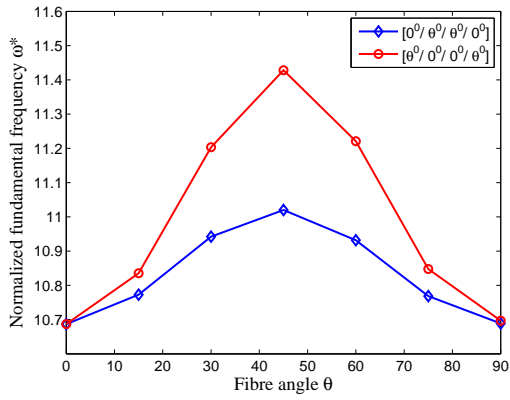
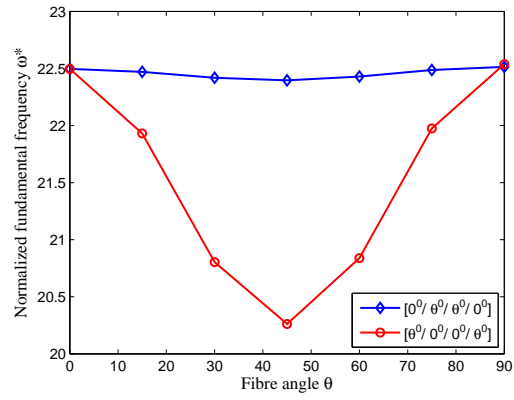


Fig. 6. Square cross-ply $[0/90/90/0]$ laminated plate: Effect of mesh distortion on the accuracy of the fundamental frequency.



(a) SSSS edge condition.



(b) CCCC edge condition.

Fig. 7. Effect of fibre orientation and stacking sequence on fundamental frequencies of square laminated plates.

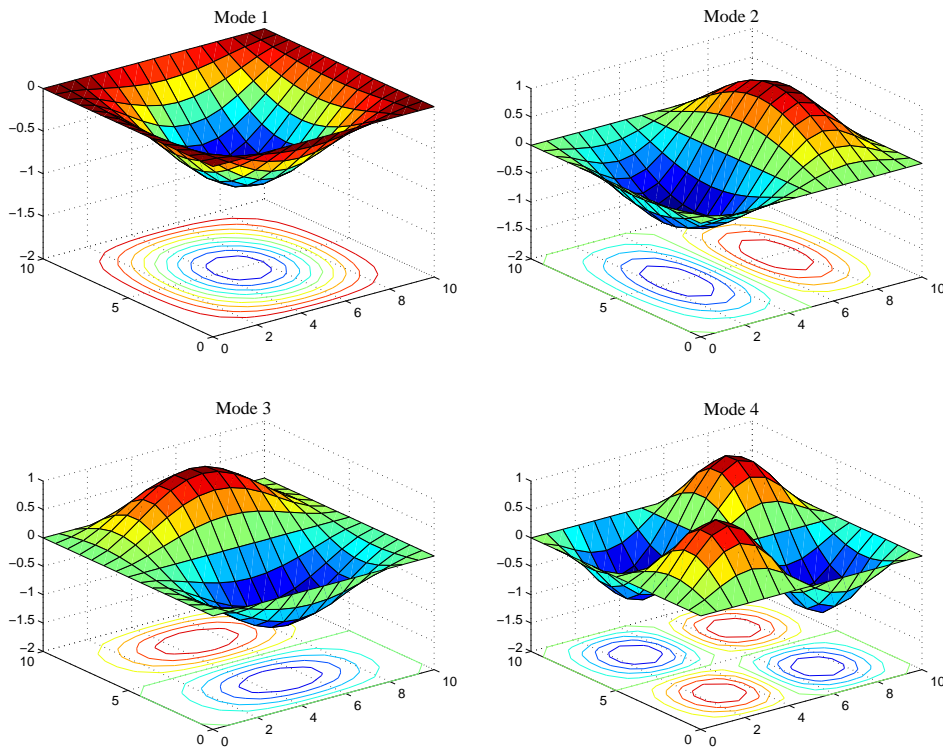


Fig. 8. Mode shapes for clamped cross-ply $[90/0/90]$ square plate ($E_1/E_2 = 40, a/h = 10$).

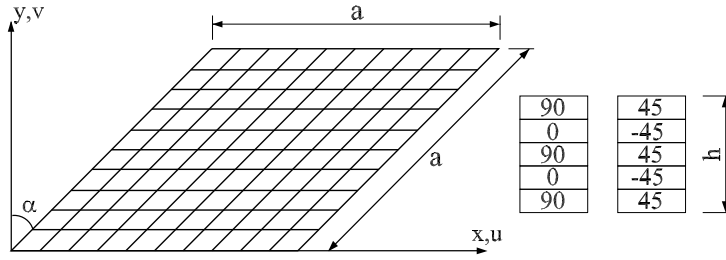


Fig. 9. Geometry and discretization of skew laminated plates

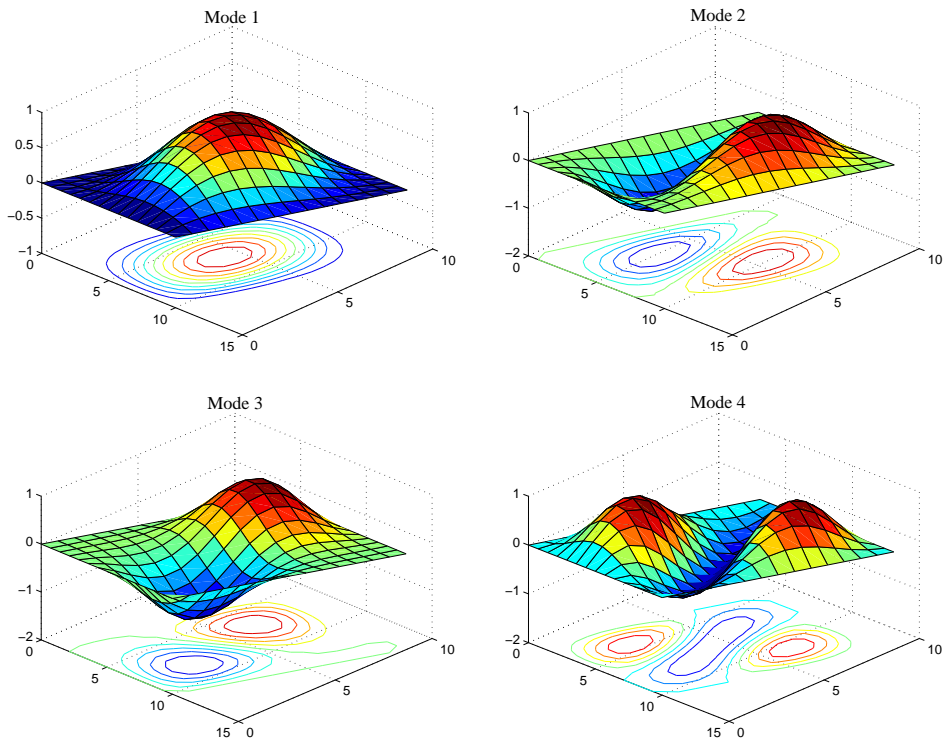


Fig. 10. Mode shapes for clamped cross-ply $[90/0/90/0/90]$ skew plate ($\alpha = 30^\circ$, $a/h = 10$, $E_1/E_2 = 40$).

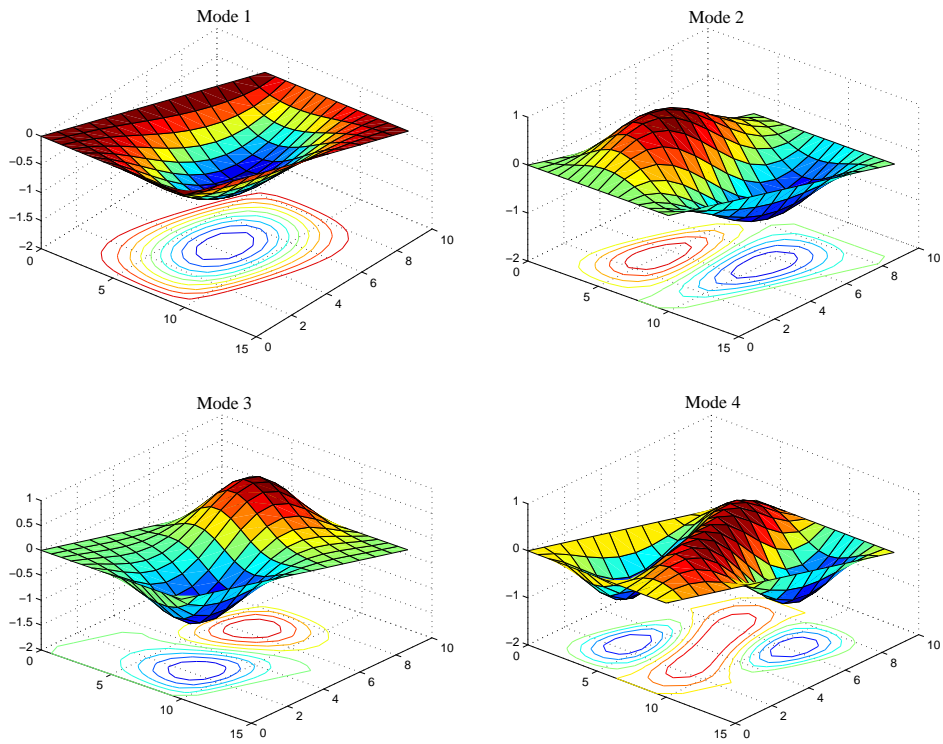


Fig. 11. Mode shapes for simply supported cross-ply $[90/0/90/0/90]$ skew plate ($\alpha = 30^\circ$, $a/h = 10$, $E_1/E_2 = 40$).

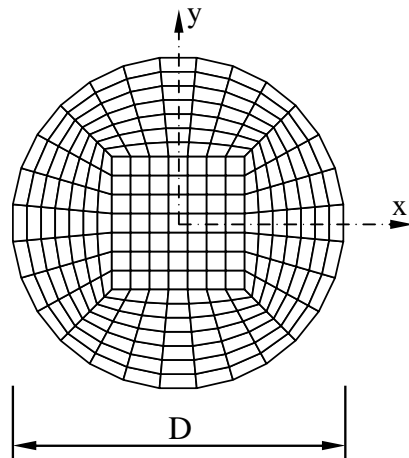


Fig. 12. Geometry and discretization of a circular laminated plate

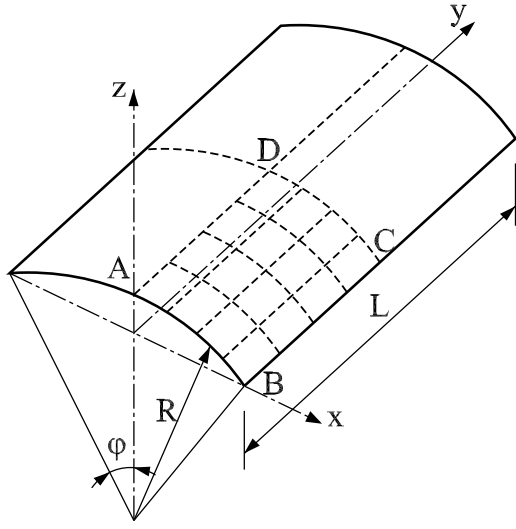


Fig. 13. Geometry and discretization of laminated cylindrical shells

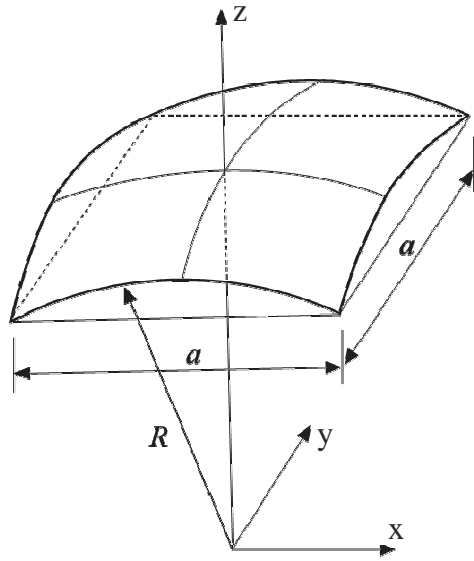


Fig. 14. Geometry data of a spherical shell